A projection technique for nonlinear adaptive analyses exploring the Generalized Finite Element Method

Bruno R.S. Souza[1], Murilo H.C. Bento[1], Sergio P.B. Proença[1]

[1]*Department of Structural Engineering, São Carlos School of Engineering, University of São Paulo*
Av. Trabalhador São-Carlense 400, 13566-590, São Carlos - SP, Brazil
brunorssouza@usp.br, m.bento@usp.br, persival@sc.usp.br

Abstract. When solving complex engineering problems of structural and solid mechanics, the adoption of linearity hypotheses may not be accurate and the use of nonlinear models can become necessary. Also, numerical methods are often used to generate approximations to them since analytical solutions are unknown for most of these problems. In this context, solving the equilibrium equations requires the use of specific strategies, with the Newton-Raphson Method being one of the most commonly adopted. In standard nonlinear analyses using the Finite Element Method, an initial solution is obtained for a first discretization. Then, the quality of this solution is evaluated to decide if further analyses are needed in order to obtain more accurate results, therefore exploring an improved discretization. If a more refined mesh is necessary, for example, the solution must be recalculated once again. In this paper, an alternative to this process is presented using a projection technique. Accordingly, all the information obtained during the analysis using a less refined discretization is transferred to the more refined one. Thus, the results provided by a first mesh is used as an initial guess for the iterative scheme in order to solve a second mesh. This also helps improving the convergence within the Newton-Raphson Method. A discussion related to the performance and effectiveness of this technique, that can be explored in combination with adaptive procedures for nonlinear analyses, is also presented. Finally, a two-dimensional geometrically nonlinear numerical problem, using the Generalized Finite Element Method, is shown to validate the presented technique.

Keywords: Nonlinear analyses, Adaptivity, Generalized Finite Element Method

1 Introduction

In practice, the use of numerical methods requires performing multiple analyses for the problem of interest in order to reach accurate enough results provided by a computational model that well represents it. Usually, an initial discretization is adopted and then its solutions are assessed to decide whether the model is adequate, i.e., whether it properly and accurately represents the problem physical conditions. The improvement of such iterative process, performed aiming at obtaining good approximate solutions, is what inspires the development of adaptive procedures. Within the context of nonlinear analyses, this iterative task can become even more computational expensive since seeking for a solution requires now solving several linear systems of equations. Following the idea previously described, an adaptive procedure that completely reprocesses a new model whenever a different discretization is built could be implemented. It is easy to see, however, that this can quickly turn the use of computational resources more expensive.

Exploiting the Generalized Finite Element Method (GFEM) ability to converge to the exact solution as the discretization is refined, an adaptive procedure that uses a previous solution already computed with a coarser mesh as a starting point for a more refined discretization can be conceived. Thus, it is no longer needed to restart the entire iterative nonlinear solution back again. The main objective is to reduce the number of iterations required for the new discretization to converge. An important step that allows performing the idea presented above is to properly project the initial solution belonging to a lower-dimensional space onto a new vector space attached to the refined mesh. Following the projection technique, the vector containing the solution obtained with the initial discretization needs to be recomputed, therefore expanded and complemented in order to fit with the new number of Degrees of Freedom (DoFs) related to the new mesh. Thus, when starting the Newton-Raphson Method (NRM),

information available from the old discretization can be used as a starting solution for the iterative procedure. This initial guess will likely be closer to the final solution than a null initial guess. The objective here is to more quickly achieve the method quadratic convergence property.

In this paper, the projection technique is presented and implementation details are discussed. In addition, this technique is applied to geometrically nonlinear numerical examples within the two-dimensional (2-D) solid mechanics context. Both advantages and disadvantages of the projection technique studied herein are also discussed. Finally, some comments on how this technique can be applied within a fully adaptive procedure are also presented.

Following this introduction, Section 2 briefly presents the nonlinear Boundary Value Problem (BVP) and the numerical method used throughout this paper. Section 3 is devoted to give theoretical aspects of the projection technique. Numerical examples are presented in Section 4, and, finally, Section 5 summarizes the main conclusions.

2 The nonlinear model problem

In this work, a geometrically nonlinear problem of solid mechanics is solved in order to evaluate the projection technique studied herein. Consider a body $\bar{\Omega} \subset \mathbb{R}^2$ with boundary $\partial\Omega$. In particular, $\partial\Omega_D$ and $\partial\Omega_N$ constitutes a partition of $\partial\Omega$, in which Dirichlet and Neumann boundary conditions are applied, respectively. The weak formulation of the BVP can be obtained by the nonlinear (total Lagrangian) description of the Principle of Virtual Work (PVW), which states:

Find the displacement $\boldsymbol{u} \in \mathscr{U} \subset (H^1(\Omega))^2$, with $\boldsymbol{u}(\partial\Omega_D) = \bar{\boldsymbol{u}}$, that solves

$$\int_\Omega \boldsymbol{S}(\boldsymbol{u}) \colon \boldsymbol{E}(\delta\boldsymbol{u}) \, \mathrm{d}S = \int_\Omega \bar{\boldsymbol{b}} \cdot \delta\boldsymbol{u} \, \mathrm{d}S + \int_{\partial\Omega_N} \bar{\boldsymbol{t}} \cdot \delta\boldsymbol{u} \, \mathrm{d}s, \tag{1}$$

for all $\delta\boldsymbol{u} \in \mathscr{U}_0 \subset (H^1(\Omega))^2$, with $\delta\boldsymbol{u}(\partial\Omega_D) = \boldsymbol{0}$.

In Eq. (1), $\boldsymbol{S}$ represents the second Piola-Kirchhoff stress tensor and $\boldsymbol{E}$ the Green-Lagrange strain tensor. The adopted constitutive law is the hyperelastic Saint-Venant-Kirchhoff (SVK) model given by $\boldsymbol{S} = \mathbb{C} \colon \boldsymbol{E}$, with $\mathbb{C}$ the 4$^{\text{th}}$-order constitutive tensor. In addition, $\bar{\boldsymbol{b}}$ and $\bar{\boldsymbol{t}}$ are body forces and tractions applied in Ω and on $\partial\Omega_N$, respectively. For detailed explanations regarding these topics, see the classical references of Bonet and Wood [1], Holzapfel [2], and Bathe [3].

The analytical solution of Eq. (1) can only be achieved in a few cases. Numerical techniques can, then, be applied in order to solve the problem. Since the problem is nonlinear, a linearization of Eq. (1) is performed and, then, a Galerkin discretization is applied to the resulting equations and so approximate solutions $\hat{\boldsymbol{u}} \in \mathscr{U}^h$ can be obtained. The finite-dimensional subspace $\mathscr{U}^h \subset \mathscr{U}$ used herein is the one spanned by GFEM shape functions.

The GFEM methodology expands the FEM approximation space by arbitrary enrichment functions in such a way that the nodes can have more functions attached to each direction in order to improve the method approximability. In addition, one of its greatest advantages is to preserve the FEM feature of using an approximation space closely related to a mesh of finite elements. A GFEM approximate displacement $\hat{\boldsymbol{u}}(\boldsymbol{x}) \in \mathscr{U}^h$ can be given by

$$\hat{\boldsymbol{u}}(\boldsymbol{x}) = \phi_{\alpha i}(\boldsymbol{x}) \, \boldsymbol{u}_{\alpha i}, \tag{2}$$

with $\alpha = 1, \ldots, n$ and $i = 1, \ldots, m(\alpha)$.

In Eq. (2), $\phi_{\alpha i}(\boldsymbol{x}) = \varphi_\alpha(\boldsymbol{x}) \, \mathcal{L}_{\alpha i}(\boldsymbol{x})$ represents a GFEM shape function, with $\varphi_\alpha(\boldsymbol{x})$ a linear or bilinear Partition of Unity (PoU) attached to the node α, and $\mathcal{L}_{\alpha i}(\boldsymbol{x})$ a scalar-valued enrichment function, with $i = 1, \ldots, m(\alpha)$ and $\mathcal{L}_{\alpha 1} = 1$. For more details about the method, see, among others, Strouboulis et al. [4], Duarte et al. [5], and Strouboulis et al. [6].

3 The projection technique

The projection technique presented herein follows the approach proposed by Thompson [7], that used the Bratu's nonlinear equation as the underlying BVP and the FEM as the numerical method to provide approximate solutions. In general, projection techniques seek to answer the following question: What is the best way to represent a vector in another space? To answer this question, these projection strategies seek to minimize the error when changing the vectors from one space to another. In the projection studied herein, two GFEM approximation spaces are involved, spanned by different discretizations, i.e., different set of shape functions.

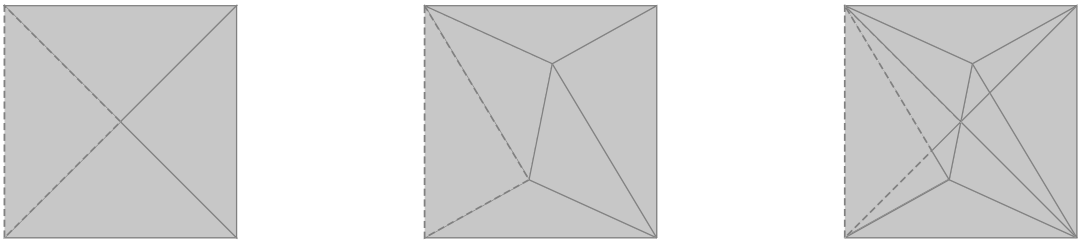

(a) Initial mesh (b) New mesh (c) Auxiliary triangulation

Figure 1. Generation of the auxiliary triangulation used for integration of the projection matrix

Starting with a solution from an initial GFEM discretization, the projection technique seeks for the optimal representation of this solution in an usually more refined discretization. Here, the set $\boldsymbol{\phi}$ contains the shape functions related to the discretization in which the solution is known, while $\boldsymbol{\psi}$ contains the shape functions related to the new discretization, obtained after one step of an adaptive procedure, for instance.

In this situation, each approximation can be given by:

$$\hat{\boldsymbol{u}}(\boldsymbol{x}) = \boldsymbol{u}_i \, \phi_i(\boldsymbol{x}) \quad \text{and} \quad \hat{\boldsymbol{u}}^p(\boldsymbol{x}) = \boldsymbol{u}_j^p \, \psi_j(\boldsymbol{x}), \tag{3}$$

with $i = 1, \ldots, \mathrm{card}(\boldsymbol{\phi})$ and $j = 1, \ldots, \mathrm{card}(\boldsymbol{\psi})$.

Using the projection technique, the coefficients that generate $\hat{\boldsymbol{u}}^p(\boldsymbol{x})$ are computed in such a way that the error $\boldsymbol{e}_u(\boldsymbol{x}) = \hat{\boldsymbol{u}}(\boldsymbol{x}) - \hat{\boldsymbol{u}}^p(\boldsymbol{x})$ be as small as possible. This can be obtained by the condition of orthogonality between the error and the subspace in which it is being projected onto. This is mathematically expressed by:

$$\langle \hat{\boldsymbol{u}} - \hat{\boldsymbol{u}}^p, \psi_k \rangle = 0, \quad \forall \, \psi_k \in \boldsymbol{\psi} \tag{4}$$

and $\langle \cdot, \cdot \rangle$ representing the standard $L^2(\Omega)$ inner product. The development of Eq. (4) yields:

$$\langle \psi_k, \psi_j \rangle \, \boldsymbol{u}_j^p = \langle \psi_k, \phi_i \rangle \, \boldsymbol{u}_i, \quad \forall \, \psi_k \in \boldsymbol{\psi}. \tag{5}$$

Finally, Eq. (5) can be written in a matrix notation as expressed in Eq. (6), in which $[\boldsymbol{M}]$ and $[\boldsymbol{P}]$ are named metric and projection matrices, respectively. According to Eq. (6), given the vector $\{\boldsymbol{u}\}$, that contains the DoFs u_i, with $i = 1, \ldots, \mathrm{card}(\boldsymbol{\phi})$, one can find the vector of projected DoFs $\{\boldsymbol{u}^p\}$, that contains u_j^p, with $j = 1, \ldots, \mathrm{card}(\boldsymbol{\psi})$, by solving the following linear system of equations:

$$[\boldsymbol{M}] \, \{\boldsymbol{u}^p\} = [\boldsymbol{P}] \, \{\boldsymbol{u}\}, \tag{6}$$

with

$$M_{kj} = \langle \psi_k, \psi_j \rangle = \int_\Omega \psi_k \, \psi_j \, \mathrm{d}S \quad \text{and} \quad P_{ki} = \langle \psi_k, \phi_i \rangle = \int_{\omega(\psi_k) \cap \omega(\phi_i)} \psi_k \, \phi_i \, \mathrm{d}S, \tag{7}$$

in which $k, j = 1, \ldots, \mathrm{card}(\boldsymbol{\psi})$, and $i = 1, \ldots, \mathrm{card}(\boldsymbol{\phi})$. In addition, $\omega(\psi_k) = \mathrm{supp}(\psi_k)$ and $\omega(\phi_i) = \mathrm{supp}(\phi_i)$ represent the support of each function.

3.1 Implementation details

The evaluation and assembly of the global $[\boldsymbol{M}]$ matrix are similar to what is applied to mass matrices within the FEM context, so no further details will be provided herein. On the other hand, the evaluation and assembly of

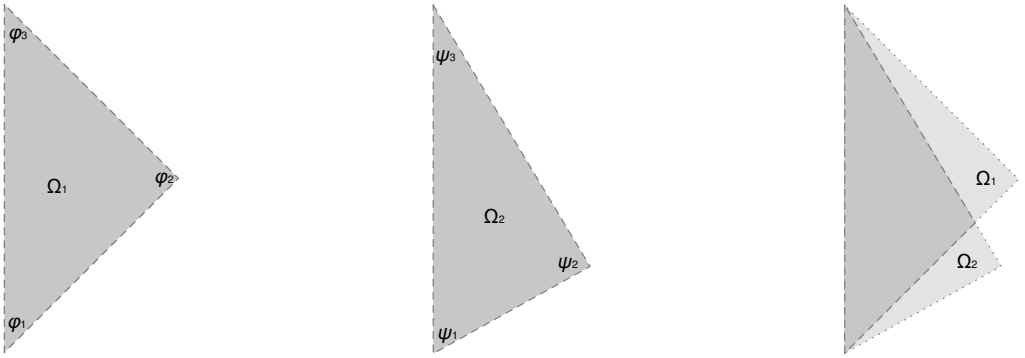

(a) Element from the mesh of Fig. 1a (b) Element from the mesh of Fig. 1b (c) Corresponding sub-element

Figure 2. Integration of local projection matrices

the projection matrix $[\boldsymbol{P}]$ demands integration over the intersection region among finite elements from two distinct meshes as shown in Eq. (7). Basically, this is necessary since the shape functions of each discretization are defined on mismatched elements.

First, to compute these intersections, an auxiliary triangulation is created. The triangles that make up this auxiliary mesh will be called, herein, as sub-elements. This triangulation is created, in this work, by algorithms provided by the CGAL Project [8]. After the generation of this auxiliary mesh, these sub-elements will act as integration domains to generate the projection matrix. To clarify this procedure, consider two distinct meshes for the same domain, as depicted in Figs. 1a and 1b. The mesh illustrated in Fig. 1c is the new auxiliary mesh created by computing the intersection of the two previous ones. The global projection matrix is, then, assembled by considering all local projection matrices computed for each sub-element. The sub-element local indexes are mapped to global indexes as in standard FEM assembly procedures.

In addition, consider that the solution is known for the mesh of Fig. 1a and that one intends to project this field onto the mesh of Fig. 1b. For simplicity, only one displacement component will be considered. When computing the local projection matrix of the sub-element highlighted in Fig. 1c, for example, all the three shape functions of the elements illustrated in Figs. 2a and 2b will be integrated over the area of the sub-element in Fig. 2c. Note that the shape functions shown in the Fig. 2 present local indexes, which is easily mapped to global ones in order to assemble the global projection matrix.

Finally, it is important to address that the method detailed before is directly compatible with linear triangular and bilinear quadrilateral elements. To compute the intersections of higher-order elements, an expansion of the algorithm presented herein needs to be done, which will be focused on forthcoming works.

3.2 On the projection and the Newton-Raphson Method

Clearly, the final DoFs projected onto the new discretization are not the final solution of the nonlinear problem. In fact, this would only happen if the problem solution is linear since the projection, in this situation, would not modify the initial vector. Usually, a null starting guess and a linear tangent matrix are chosen when seeking for a solution by using the Newton-Raphson Method. However, this guess is often too far from the solution of the nonlinear problem and, because of this fact, it is necessary a large number of iterations to achieve the convergence. Therefore, the applicability of this technique aims at using the projected solution as an initial guess instead of the linear one, supposing it will be closer to the final solution when solving the problem in the finer mesh. The initial tangent matrix is also improved.

Another important feature to be reminded is related to the Newton-Raphson Method quadratic rate of convergence, reached as the iterations get closer to the solution. Therefore, the projection technique, by providing an initial guess closer to the final solution, contributes to more quickly reach the previously mentioned convergence property. The property can be expressed by

$$\|\boldsymbol{u} - \hat{\boldsymbol{u}}_{n+1}\|_{L^2(\Omega)} \leq C \, \|\boldsymbol{u} - \hat{\boldsymbol{u}}_{n}\|^2_{L^2(\Omega)}, \tag{8}$$

with $C > 0$ a constant.

4 Numerical example

4.1 Problem description

The example chosen to demonstrate the efficacy of the projection technique consists of a cantilever beam under a bending moment load, that is imposed through a linear traction applied at its free end. Fig. 3 shows the beam geometry and boundary conditions. A Young's modulus $E = 2 \times 10^8$ and a Poisson's ratio $\nu = 0.3$ are assumed. In the region where Dirichlet boundary conditions are enforced, a Young's modulus ten times higher than the one adopted elsewhere is assumed in order to prevent some numerical instabilities related to geometrically nonlinear analyses. Moreover, plane stress conditions are adopted. Finally, the stopping criteria for the NRM is $\|R^{(k)}\|_2 \,/\, \|R^{(0)}\|_2 < 10^{-10}$, with $\|R^{(k)}\|_2$ the L^2 norm of the residual vector for the (k)-th iteration.

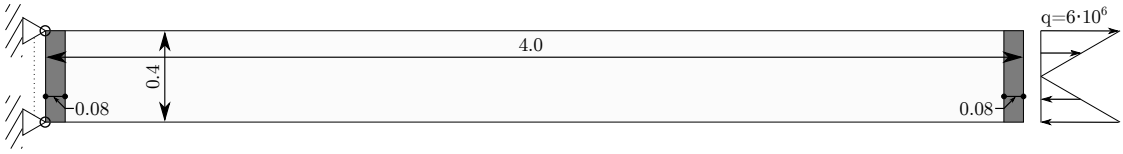

Figure 3. Problem description

To study the projection technique presented herein, two different initial mesh topologies are analyzed. In the first set of simulations (Case 1), a structured mesh is adopted with bilinear quadrilateral elements (see Fig. 4a). A more refined mesh with the same element type is then used to simulate an *h*-adaptive process (see Fig. 4b). In this case, no enrichment is adopted, recovering, then, FEM approximate solutions.

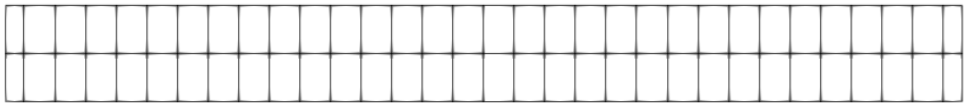

(a) Initial mesh

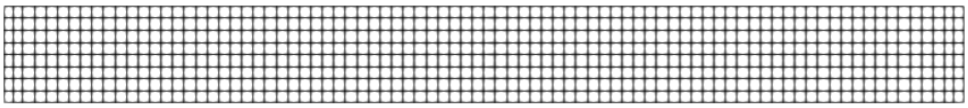

(b) New mesh

Figure 4. Initial and new meshes - Case 1

In the second set of simulations (Case 2), an structured mesh is also initially adopted, however using linear triangular elements (see Fig. 5). To simulate a *p*-adaptive process within the GFEM context, a new discretization is generated by enriching all the nodes of the initial mesh in each direction by the set of polynomial functions $\mathcal{L}_{\alpha i} \in \{1, p^{1,0}, p^{0,1}\}$, with

$$p^{i,j} = \frac{(x - x_\alpha)^i \, (y - y_\alpha)^j}{h_\alpha^{i+j}}, \tag{9}$$

and x_α and y_α the coordinates of the enriched node α. In addition, h_α is defined as the greatest distance between this same node and its neighboring nodes.

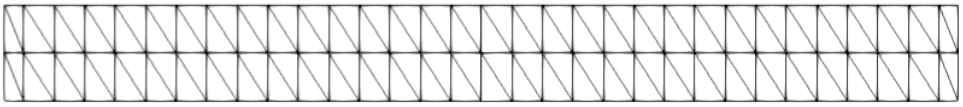

Figure 5. Initial mesh - Case 2

4.2 Results and discussion

For both Cases 1 and 2, the coarser meshes are solved using 10 load steps. After the convergence of each step, in which the deformed shapes are depicted in Fig. 6, a projection of the current solution onto the finer mesh is done. As already specified in Section 3, this projected solution is used as an initial guess to the NRM when solving the more refined discretization. This more refined discretization is solved with only 1 load step.

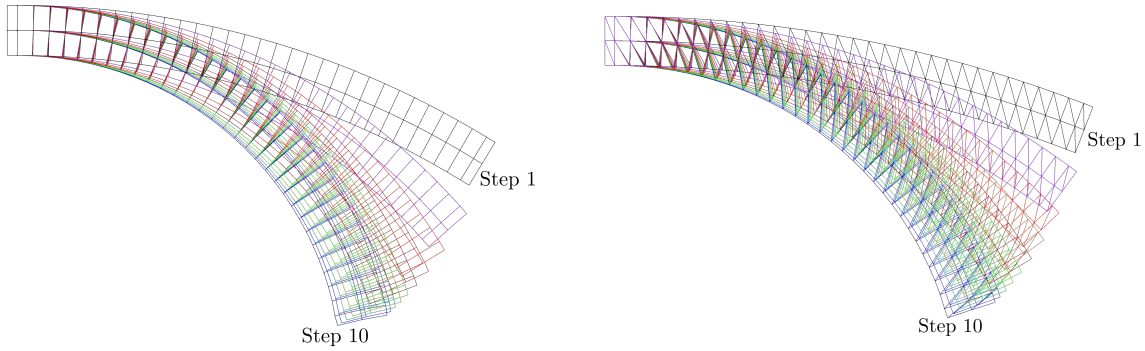

(a) Case 1 (b) Case 2

Figure 6. Deformed shapes for each step of the initial discretizations

The convergence behavior along the NRM iterations for the more refined discretizations is shown in Fig. 7 for all the initial guesses provided by every load step of Cases 1 (Fig. 7a) and 2 (Fig. 7b). Two general observations are made about it. First, the black solid curves with initial null guesses (named "No Projection") are used herein only to compare the improvements when initial guesses, computed with the projection technique, are adopted. Second, the initial value of the L^2 norm of the residual vectors almost coincides for all curves since, in this case, $\|R^{(0)}\|_2$ depends mainly on the imposed traction load.

Moreover, the plots depicted in Fig. 7 show that in the last iterations of all analyses the curves become almost parallel. This indicates that an optimal rate of convergence is reached. An important fact to be highlighted here is that the number of iterations to reach this optimal rate of convergence significantly decreased as the projection is done using final solutions of the coarser mesh. This shows that the projection technique can indeed take advantage of these improved initial guesses.

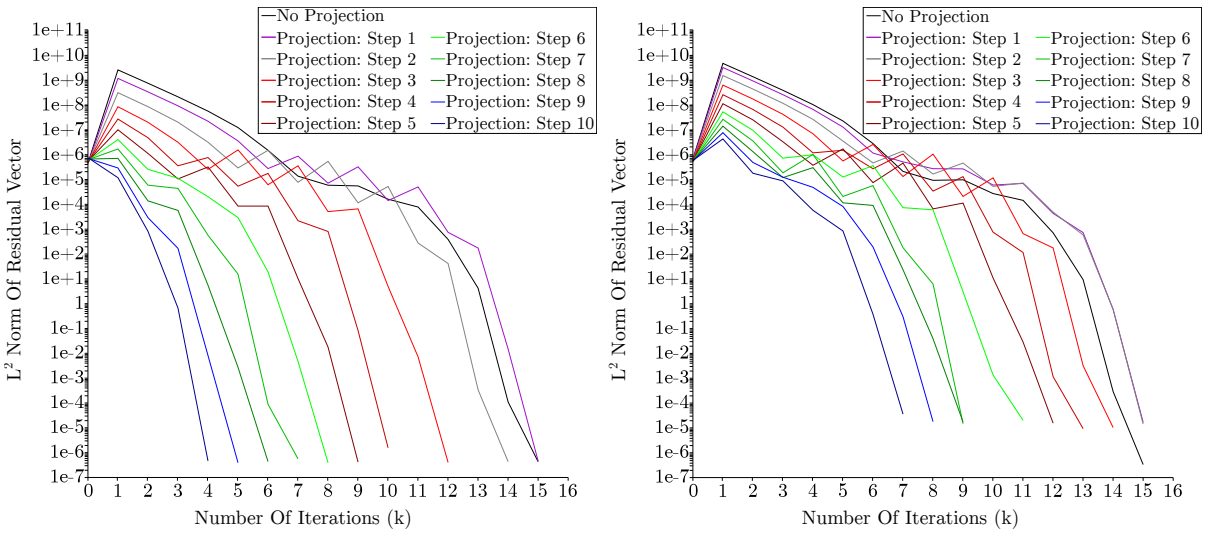

(a) Case 1 (b) Case 2

Figure 7. Convergence of the more refined discretization after projecting each load step of the initial discretization

It can also be observed that in the first step of both Cases 1 and 2 the provided initial guess does not bring improvements to the NRM. This indicates that the projection technique must be used carefully since some initial

guesses bring little or no improvement to the NRM convergence behavior. However, using initial guesses closer to the final solution strongly improves the method convergence, as shown in Fig. 7.

Comparing both Cases 1 and 2 in Table 1, it can be noticed that, in Case 1, the projection technique may continuously decrease the number of iterations in a limit from 17 to only 4, with a relative gain of approximately 73%, while in the second the best relative gain was approximately 53%. Although both coarser meshes have the same number of DoFs, the difference on the relative gains happens because the last case is solved using linear triangular elements, which have, in general, less quality of approximation than the bilinear quadrilateral elements. Because of this, poorer solutions are obtained, yielding then poorer initial guesses.

Table 1. Number of iterations (NI) and relative gain (RG) for each load step (LS)

LS	NI		RG (%)	
	Case 1	Case 2	Case 1	Case 2
1	15	15	0	0
2	14	15	7	0
3	12	14	20	7
4	10	13	33	13
5	9	12	40	20
6	8	11	47	27
7	7	9	53	40
8	6	9	60	40
9	5	8	67	47
10	4	7	73	53

5 Conclusions

The projection technique presented herein shows to be promising to be used along with adaptive procedures for nonlinear analyses of solids and structures performed by either the FEM or the GFEM. Using this technique, it was illustrated that problems with projected initial guesses need fewer iterations to reach the convergence when solved by the Newton-Raphson Method than when a null initial guess is adopted. This also helps to more quickly achieve quadratic convergence. Forthcoming works will focus on fully adaptive procedures for nonlinear problems with this technique being adopted to transfer information between discretizations, which is required to accomplish this type of analyses.

Acknowledgements. The authors would like to acknowledge the support of the University of São Paulo (USP). This study was financed in part by the Coordenação de Aperfeiçoamento de Pessoal de Nível Superior – Brasil (CAPES) – Finance Code 001.

Authorship statement. The authors hereby confirm that they are the sole liable persons responsible for the authorship of this work, and that all material that has been herein included as part of the present paper is either the property (and authorship) of the authors, or has the permission of the owners to be included here.

References

[1] J. Bonet and R. D. Wood. *Nonlinear continuum mechanics for finite element analysis*, volume 1. Cambridge University Press, 2 edition, 2008.
[2] G. A. Holzapfel. *Nonlinear solid mechanics : a continuum approach for engineering*. John Wiley & Sons, 1 edition, 2000.
[3] K. J. Bathe. *Finite element procedures*. K. J. Bathe, 2 edition, 2014.
[4] T. Strouboulis, I. Babuška, and K. Copps. The design and analysis of the generalized finite element method. *Computer Methods in Applied Mechanics and Engineering*, vol. 181, n. 1-3, pp. 43–69, 2000.
[5] C. Duarte, I. Babuška, and J. Oden. Generalized finite element methods for three-dimensional structural mechanics problems. *Computers & Structures*, vol. 77, pp. 215–232, 2000.
[6] T. Strouboulis, K. Copps, and I. Babuška. Computational mechanics advances. the generalized finite element method. *Computer Methods in Applied Mechanics and Engineering*, vol. 190, n. 32-33, pp. 4081–4193, 2001.
[7] R. A. Thompson. Galerkin projections between finite element spaces. Master's thesis, Faculty of the Virginia Polytechnic Institute and State University, Virginia, 2015.
[8] The CGAL Project. *CGAL User and Reference Manual*. CGAL Editorial Board, 5.3 edition, 2021.